MONTE CARLO IRRADIATION MODEL FOR LONG-TERM LOW DOSE ENVIRONMENTS FOR SPACE LIFE SCIENCE APPLICATIONS

A Thesis

by

DAVID HAMILTON SAUCIER

Submitted to the Office of Graduate and Professional Studies of
Texas A&M University
in partial fulfillment of the requirements for the degree of

MASTER OF SCIENCE

Chair of Committee,	John Ford
Committee Members,	Susan Bloomfield
	John Poston
Head of Department,	Yassin Hassan

May 2016

Major Subject: Nuclear Engineering

ABSTRACT

This research looks at the intersection of computational methods in radiation transport and biological experimentation. An essentially zero-cost metric (with the exception of relatively low time cost) or estimate for an experimental procedure for irradiation planning can help optimize the dose, shielding, and geometrical considerations. The motivation of this research is to provide a comprehensive Monte Carlo model for use in a long-term, continuous low-dose irradiation experiment on hind-limb unloaded rodents. This model presents data on experiment-exact source models and exact room geometries to meet the strict dose, cost, and shielding requirements. The method for answering these metrics will be through statistical or Monte Carlo radiation transport with the overarching goal of this project being not only to offer data to compare with physical radiation experiments, but also to determine if this type of method holds promise in long-term, low-dose experiments for radio-biological studies.

The determined optimum geometry was the star geometry with sand collimators and lead shielding on the wall hot-spots. This met dose requirements inside and outside the room while fitting into the budget of the experiment.

NOMENCLATURE

PTA	Peak-To-Average Flux in Rat Cage
TAMU	Texas A&M University
HODR	Highest Outside Dose Rate (mrem/hr)
ENDF	Evaluated Nuclear Data File
NIST	National Institute of Standards and Technology
$\dot{D}$	Dose Rate (mrem/hr)

TABLE OF CONTENTS

Page

LIST OF FIGURES

FIGURE Page

LIST OF TABLES

TABLE Page

1. INTRODUCTION: MONTE CARLO METHODS AND RADIATION INTERACTIONS WITH SHIELDING

This thesis research provides valuable data to a physical experiment utilizing statistical computational methods. Many experimental institutions are seeing the benefits of using computational simulations before implementing experiments to provide preliminary data for the viability of the experiment. This particular experiment addresses two important arenas: radiation safety and radiation biology experiment planning.

1.1 The Physical Experiment

The live-animal experiment is looking at the long-term, continuous low-dose effects on hind-limb unloaded mice. These mice will be put in a rat cage assembly and have a geometry of Cobalt-60 wire sources surrounding them with the hind limbs in a sling to simulate micro gravity on the legs. The total activity of the sources will be set such that an integrated dose equivalent of the dose rate will be equal to 0.5 Gy. The equation below illustrates this principle of integrating the dose-rate.

$$\int_{t_0}^{t} \dot{D}(\frac{mrem}{hr})dt \tag{1.1}$$

Where $\dot{D}$ is the dose rate, t_0 is the starting irradiation time and, t is the time irradiation stops. To accurately account for the effects that the astronaut's body see from radiation, something called a dose equivalent is used. This dose equivalent looks at the radiation particle time (and its energy for neutrons) and assigns it a quality factor 'Q' or weighting factor 'w_t.' This factor serves as a 'weight' to show how much effective dose is given biologically. For example: 1 Gy of α dose is 10-20

times more effective than 1 Gy of γ radiation. To avoid confusion, a change of units is given in radiation to show how much effective dose is given, the Sievert and rem. They are converted from Grey and rad respectively by simply multiplying by the weighting or quality factor. [7] This is shown in the following equation:

$$\dot{D}_{effective}(Sieverts) = Q_{particle}\dot{D}(Grey) \tag{1.2}$$

where $\dot{D}_{effective}$ is the effective dose rate, $Q_{particle}$ is the weight for the given particle, and $\dot{D}$ is the un-weighted dose rate. This equation is used to ensure that the dose we give the mice matches what astronauts are seeing, 0.5 Sieverts. Using this, we determine we need an integrated dose of 0.5 Gy of γ irradiation (because the $Q_{gamma} = 1$.) Assuming this required dose, 22 hours of irradiation a day, and that there are 28 days for irradiation a dose rate of $83\frac{mrem}{hr}$ is required.

Cobalt 60 is chosen for the source material because of the energy spectra. The 1.1 and 1.3 MeV gammas help mimic the main contributor to dose in space, δ rays. Delta rays are scattered electrons generated from more energetic radiation (commonly α particles scattering electrons from their atomic orbitals with relatively high energy. These, in turn, can interact directly on the DNA or indirectly through creating reactive oxygen intermediates (ROS). Radiation interactions can therefore disturb cell functions and even cause apoptosis of the cell.

Low-dose effects data represent a very small portion in radiation effects. It is still unknown what the exact effects are biologically at low dose rates be they beneficial (hormesis) or detrimental. This experiment gathers data in this arena as well as data for astronauts in the International Space Station to help characterize what

is happening to overall bone health as well as the effects of iron-oxidation overload. The results of this live-animal experiment contribute knowledge these arenas and will be instrumental in helping determine low-dose effects *in vivo* and in microgravity. [2]

1.2 The Digital Design: What is Monte Carlo?

Monte Carlo radiation transport methods have been used extensively in the nuclear engineering arena since the early 1940s. It allowed an alternative to time-consuming hand calculations that allowed for more advanced geometry input passed simple shapes like cylinders and boxes. Since then, the merit of these models has been recognized even further with the advent of increased computational power. Correspondingly so, the overall usefulness of Monte Carlo methods have gone up considerably as most experiments may be simulated on a home computer in comparison with the computers that would take up entire rooms in the early days of nuclear engineering. This translates to an increase in availability of Monte Carlo to all arenas of research and development. [1]

Statistics lie at the center of Monte Carlo methods. By introducing a large number of random interactions into a given system, the probabilistic distribution of nearly any system may be obtained. In the case of this experiment, we are generating Cobalt-60 photons with a equally probable solid angle in a full 4π steradian space. These photons go on their own 'walk' and have a statistical probability of interaction whenever a new material is encountered. If enough particle histories are completed, and the results of their walk compiled, valuable estimates of fluence-rate and corresponding dose may be given.

At its essence, this research seeks to hybridize the technology and tools of nuclear engineering with radiation biology. Monte Carlo statistical radiation transport can create complex models to estimate doses to experiments using exact environmental characteristics. [1]

1.3 Alternative Methods

Another primary method alongside Monte Carlo is deterministic transport. Deterministic methods are beneficial for fast calculations. They rely on simplifying radiation sources and room materials into very simple shapes, like a cylinder or cube. Deterministic codes center around using a simple geometry to simplify a difficult transport equation, but solve it exactly. Conversely, Monte Carlo simulations use statistics and interaction probabilities to get an non-exact answer. Mathematically, to get a Monte Carlo result with no uncertainty would mean running a computational simulation for an infinite amount of time. [1] [7]

For this research, complex source geometries are necessary. Monte Carlo simulations allow a high degree of complexity in geometry of the source and target, at the cost of not having an exact answer like the ones given with deterministic methods. This statistical error given in Monte Carlo calculations is directly related to the number of particle histories. Thus, to get a reasonable statistical value, more histories must be run and correspondingly, more time is needed for each simulation. Despite this, Monte Carlo is the right choice for this research thesis as it offers valuable data in the complex source geometry. However, it should be noted that deterministic methods are increasing their capabilities by leaps and bounds, but complex lattice or geometry input generates very complex equations to be solved which may or may

not be outside the scope of the code and its assumptions. [6]

The final alternative is hand calculations. This can be done, but the time it would take for each iteration would be much greater than creating a deterministic model or even running a suite of Monte Carlo runs. Although this might be feasible for experiments that use one relatively simple geometry, this is not a possibility for this experiment as there are many geometry orientations with complex geometry modeling.

1.4 Radiation Shielding and Interactions

This section outlines the physics behind photon interactions with matter that are important to the shielding design for this experiment. Concepts such as attenuation and buildup factors are introduced to help explain the physics as well as offer up information that can be used to validate this radiation model.

1.4.1 Photon Interactions

Photons can interact in three ways with matter. The first is the photoelectric effect, which takes place at lower energies from 0.01- 0.1 MeV. Compton scattering is another effect that dominates in the region of 0.1-5.0 MeV. The final interaction is pair production and can happen at any energy above 1.022 MeV. A visual diagram depicted on Fig. 1 depicts the energy-dependence of each interaction. [7]

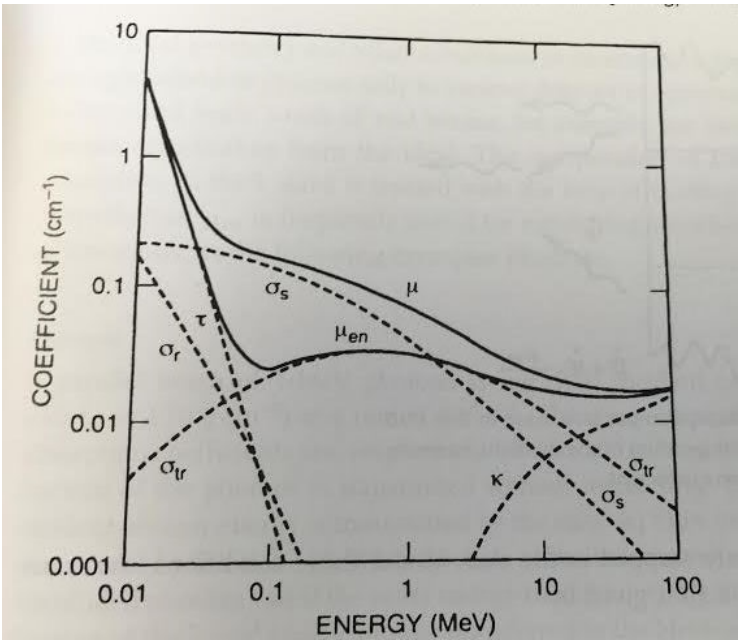

Figure 1.1: Probability of each photon interaction with respect to energy taken from Turner [7]. Here κ is the pair production probability, σ_f is the photoelectric effect probability, σ_s is the Compton scattering probability, and μ is the total photon attenuation coefficient used for shielding calculations. The other variables are not of interest for the purpose of this research.

The probabilities shown in the above graph are known as attenuation factors. They may be used in determining the right shielding for a system. A metric of interest is the mean free path (MFP), which is shown below in Eqn (1.3):[4]

$$MFP = \frac{1}{\mu_{total}} \tag{1.3}$$

where μ_{total} is the total interaction probability from each of the three interactions, hereafter referred to as μ. The mean free path is defined as the average particle track length traversed by a photon of energy, E , across a material of a given number

density. These metrics give an idea of which shielding materials would be best to use for a given experiment that might have cost, size, or other special considerations. For the purpose of this project, lead and sand were the chosen two shielding materials. Lead was chosen for its high attenuation coefficient and sand for its low cost and ease of molding into different shapes.

1.4.2 Photon Shielding: Energy Dependence and Buildup Factors

Photon interactions are characterized by their mass energy attenuation coefficients. These are energy-dependent values that are quantified for a given shielding material of interest. Assuming a mono-directional beam of photons, the fluence rate at a distance 'x' in a given material can be described using Eqn. 1.4.[6]

$$I(x) = I_0 e^{-\mu x} \tag{1.4}$$

Where I_0 is the starting fluence rate, μ is the total attenuation coefficient, and x is the distance the photon travels in the material.

This equation changes when the geometric considerations change from a simple mono-directional source to a isotropic source interacting with the walls of a room or with objects such as a rat cage. In order to account for this, a term called the build-up factor is introduced (B_0), and the resulting equation is Eqn. 1.5.

$$I(x) = B_0 I_0 e^{-B_0 \mu x} \tag{1.5}$$

When validating the model in later chapters, it will become evident that our model will have shielding in-scatter effects, yielding a buildup factor. An approxi-

mate B_0 for a large lead shield at an average energy from the two Cobalt-60 gammas is 1.08 [6]. This value will be compared to the one obtained from the model as well as the published attenuation factor from NIST. This, along with checking for back scattering effects, will serve as physical checks that the physics of the model are working properly.[3]

Currently, a review of the literature has revealed no other experimentation or computational work that could serve to further validate this model. Accuracy of this model will be analyzed through comparison of in-cage rodent dosimetry with the results taken from this MCNP6 model. Some deviation is expected because the results from this model give the most conservative dose to the outside rooms based on a experiment required source activity.

2. PARAMETRIC STUDIES USING MONTE CARLO

This research looks at a variety of cases that all look at different source orientations and shielding designs. To optimize each step, a scope had to be defined, parameters made, and a method generated.

2.1 Scope of Research

From the research description given in the previous section, the following items are defined to show what is expected of the model:

- An optimized source & collimated geometry delivering:
  - [+] Average dose of at least 83 $\frac{mrem}{hr}$ for each rodent cell
  - [+] No dose response higher than 2 mrem/hr outside room
- A reproducible model that can change source geometries or dimensions easily

These requirements define the scope of this project. Within each of these are further checks and balances that had to be made with each parameter study. These balances are given below:

1 Make sure dose limits are maintained for workers and people

  [a] For long ($\approx$ 60 day) exposure, ensure chronic dose is acceptable

2 Dosage to rodents meets experimental needs

  [a] Receives dose accurate of a 30-60 day NASA mission (ex. Mars)

  [b] Accurately reflect the combined effects of radiation and gravity

To balance both the shielding and experimental needs, a process was devised that would iterate through a series of five geometries to meet the requirements and maximize the benefits for the experimenters. The process is outlined in Fig. 2.1. Once this process flow was defined, the geometry, building geometry, materials and dose calculation methods had to be created in the Monte Carlo code. The overarching goal of this being a possible metric for experiment planning. Success in this research could lead to this method being applied in a wider range of applications.

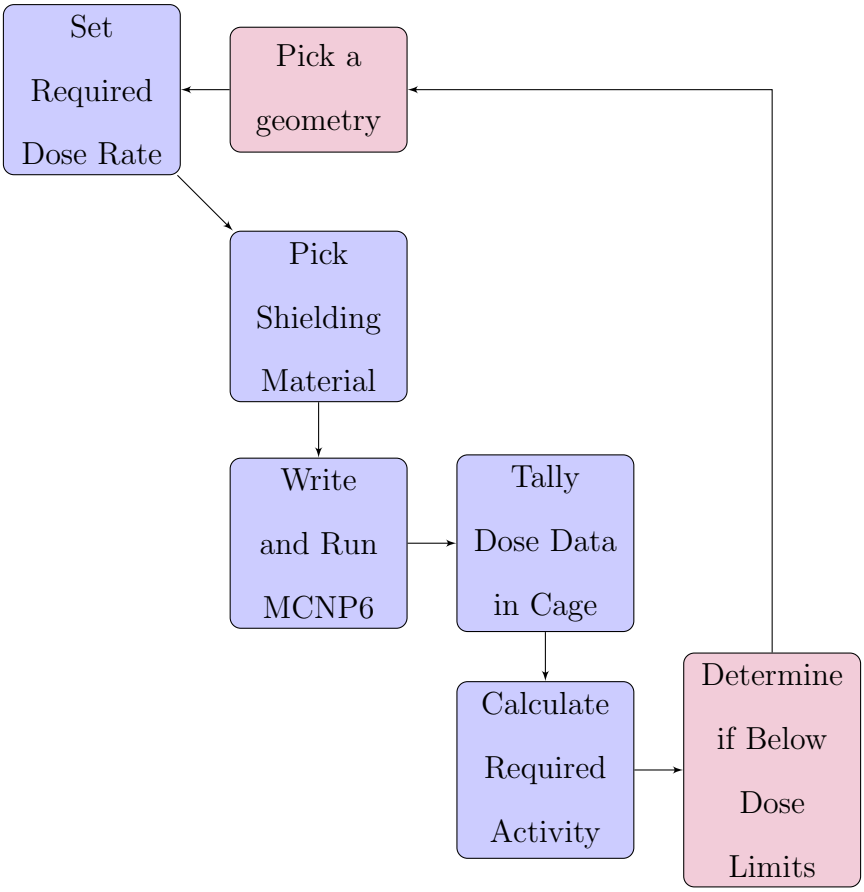

Figure 2.1: Flowchart to determine optimum source geometry.

2.2 Making the Method

The computational code used for this research will be the Monte Carlo N-Particle Program 6 (MCNP6), which is currently used for a myriad of applications in the nuclear engineering field ranging from nuclear criticality safety to medical physics. The chief reason for using this code over other Monte Carlo codes is because of the readily available response functions for photons as well as the author's experience with the code. In addition, there was a large variety of literature available to help in the generation of the source geometry.

2.2.1 Source Modeling

Complex source modeling is made possible through MCNP6 and various publications give examples for methods that may be applied to ensure proper physics and sampling of the source geometry. The two methods of interest for this project are parallelipiped sampling rejection and source cell sampling. These methods, when used in conjunction, may be used to create any manner of source geometry. The method works by defining a bounding box around the cells of interest (the source cells). The code will then sample values inside both the bounding box and in the source cell. The sampling is completely random and will sample for a given position and direction track, keeping in mind all angles are probable. This method which is the backbone of Monte Carlo, allows for essentially any source to be used. [1]

Initial-run source geometries were chosen because they offered ideal homogenized radiation flux across all of the rodent cages. Dose rate to the outside rooms were controlled by the addition of collimators or decreasing number of sources to ensure dose rates are below the limits set in the objectives. Prior to adding collimators, a

'baseline' case will be run. The purpose will be to gather physics information in the form of fluence rate and dose rate to generate an attenuation curve for lead. This value will be compared to NIST to ensure the source physics are acting to expectations.

In all, there were five total source geometries used for this experiment. Others were eliminated from the trial list on the first-run for having either too high of a dose rate, or a very high peak-to-average flux inside the rodent cages.

2.2.2 Geometry

Specific room parameters were taken from the drafting drawings of the actual building to ensure accuracy of the rodent experiment. The surrounding spaces, hallways and tangential rooms were input into the model. The drafting drawings gave immense amount of detail on the doorways, floor thicknesses, and walls that allowed for an incredibly realistic computational representation. Of equal importance was that the drawings also specified the shielding in the walls in terms of a thickness of lead shielding.

To confirm that the physics (particle scattering, attenuation of photons) of the modelled room was being properly done in the model, of interest was the buildup factor. Theoretical values for a room with an infinite lead shield give values of 1.08 for Cobalt-60 gamma rays. [6] To confirm the geometry is contributing the right physics, the model value for a buildup factor is compared to this value. Deviations were expected, as this research looked at lead shielding thicknesses of 1-20 mm when generating dose data and not an infinite shield of lead around the room.

2.2.3 Materials

Accurate material characteristics are needed, as they are what will provide the relevant interaction probabilities or nuclear cross sections. The cross sections will be selected for a room temperature environment of roughly 20° C from the latest ENDFVII cross section library for photons. These cross sections shall be used for each isotope present in the materials of interest for this model.

Composite materials' composition shall be taken from the PNNL Materials compendium data base [5]. These material compositions have been used extensively in computational transport and specifically in MCNP6 simulations. This resource will be of use for generating material cards for concrete, sand, wood, and other materials of interest that could serve to optimize the source geometry problem.

2.3 Calculating the Dose

Dose is limited by the required dose rate needed for the experiment (83 $\frac{mrem}{hr}$). This dose rate is assumed and compared with the dose response in the rodent cages. These dose responses are found by taking the particle flux in a 'rodent detector' the rough size and shape of a rodent and determining the dose response through energy-dependent response functions.

Response functions are an integral part of these dose calculations and are a function of energy and particle type. Dose is obtained, per source particle, by multiplying

a response function to a particle track length flux tally (Eqn. 2.1). [7] [6]

$$\dot{D}(\frac{mrem}{hr * photon}) = R(E)\phi(r, E) \tag{2.1}$$

Where $\dot{D}$ is the response rate, $R(E)$ is the energy-dependent response function and $\phi(r, E)$ is the particle track-length flux. From the units, it can be discerned that the total dose acquired must be multiplied by a source strength to be in units of dose rate. What is applied here is another formula to solve for the required activity, assuming a dose rate, given by Eqn (2.2). The assumed dose rate in this case is the one required to meet the objectives of the experiment: 83 $\frac{mrem}{hr}$.

$$A_{required} = \frac{\dot{D}_{required}}{R(E)} \tag{2.2}$$

This activity, $A_{required}$, can then be used with the detector tallies outside the room to calculate the dose in the surrounding areas and ensure that it is smaller than 2 $\frac{mrem}{hr}$. This is calculated using Eqn. 2.3 below.

$$\dot{D}_{outsideRoom} = A_{required}R(E)_{outsideDetectors} \tag{2.3}$$

These equations shall be iterated upon and solved for each source geometry situation to determine which of them meet the requirements set earlier in the objectives. These data shall then be given to the experimenters to determine which source geometry would offer the best benefits.

2.4 Validating the Model

When the lead shielding trials were complete, the calculated attenuation factor for the model was 0.073 cm^{-1} (Fig. 2.2) which was off by 10.8% from the published

NIST value of 0.0607. From theoretical expectations, there should be a deviation from the attenuation value because of additional backscattering from the model geometry (a buildup factor.) Assuming this difference is due to the buildup factor, the calculated buildup factor is 1.20 for the experimental geometry, which is in the ballpark of the theoretical value of 1.08, corresponding to a 10% difference. Because the statistical uncertainty in the MCNP data was $< 2\%$ and the values were relatively close to the published values, the physics of this model were deemed to be effective at modeling the source and dose response outside the room.

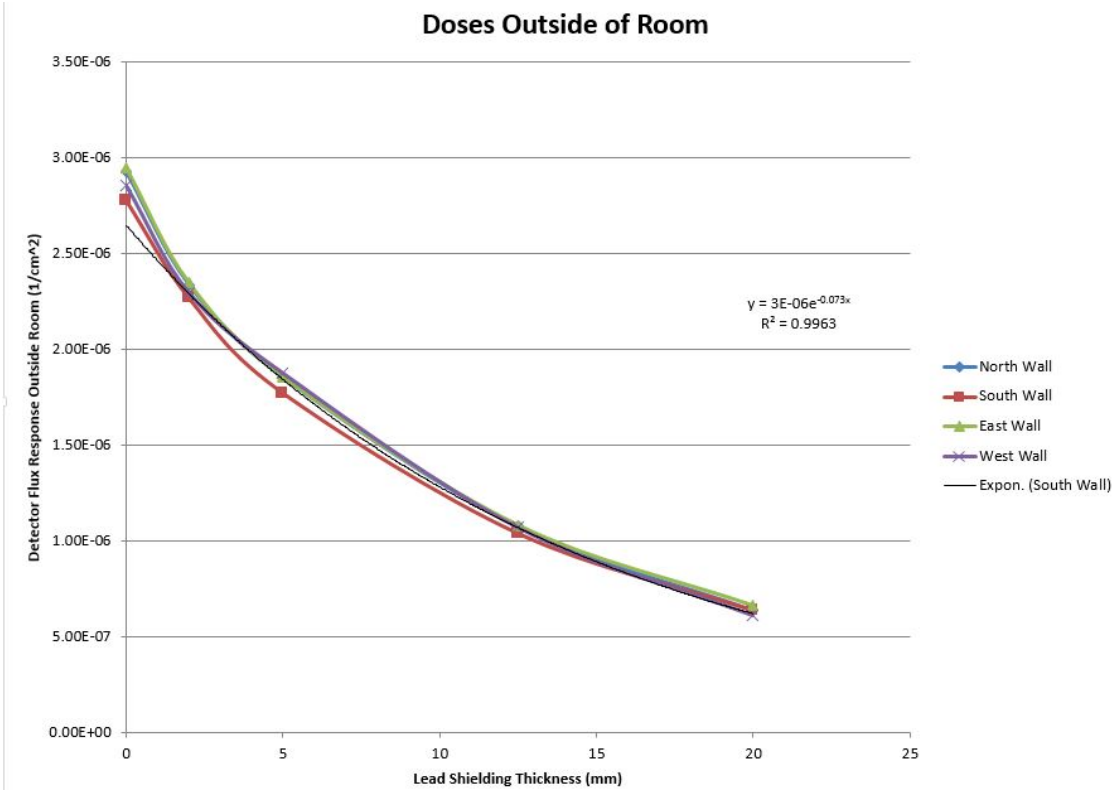

Figure 2.2: Graph of photon attenuation as a function of lead shielding thickness for baseline model. The label 'Expon. (South Wall)' is a exponential trendline fit to show the attenuation factor in the exponential term, 0.073 cm^{-1}.

Another check of the model was to observe changes or anomalies in the fluence rate inside of the rat cage as lead shielding was added. The addition of lead shielding causes more gammas to reflect back into the system, so a corresponding increase in fluence rate must be observed as more shielding is added. This is shown on Fig. 2.3 and meets theoretical expectations.

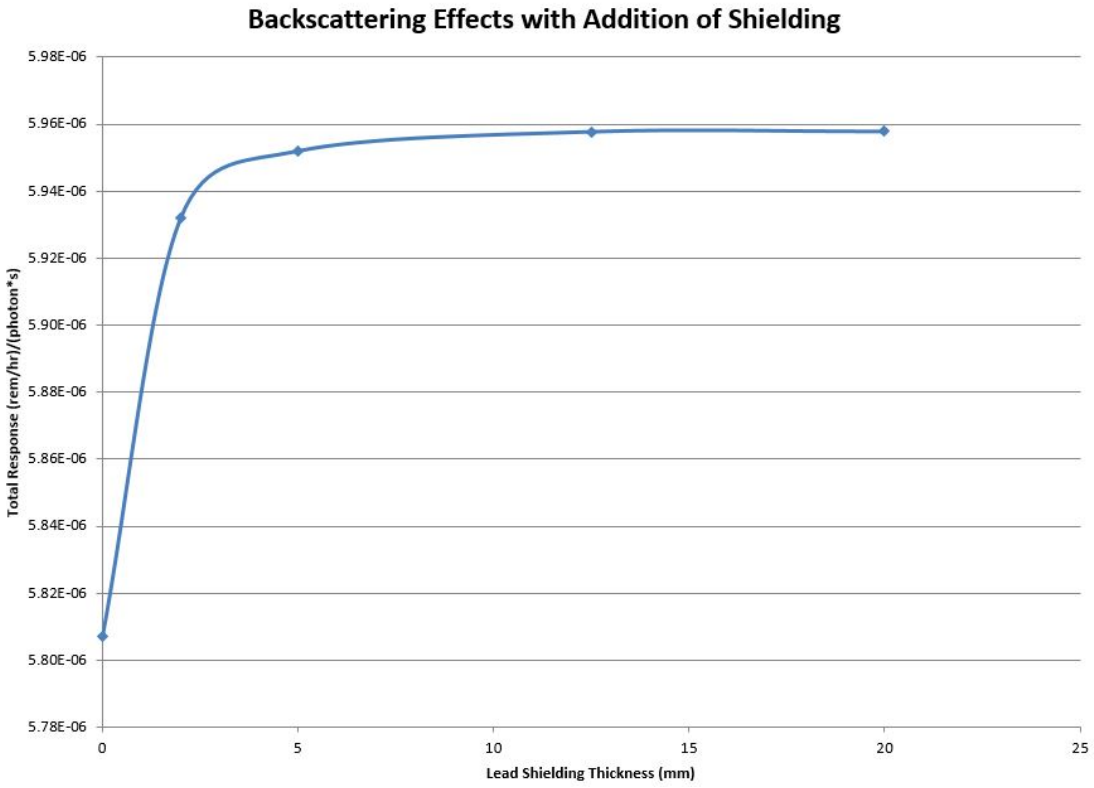

Figure 2.3: Physical check to see if backscatter into the irradiation room increases with addition of shielding.

3. RESULTS AND ANALYSIS OF MONTE CARLO MODELS

Results for each of the 5 primary geometries is presented in this chapter. Relevant data includes: required source activity, received dose outside the room, peak to average flux inside of the rat cage and, finally, any relevant shielding information. Cases start as very general source orientations and are iterated upon to better fit the needs of the experimenters. Tables 3.1 and 3.2 contain a summary of all the relevant data for each of the individual geometries.

3.1 Geometries Used

Each of the five geometries are given below. The various advantages and disadvantages of each are discussed and results presented at tables at the end of this section.

3.1.1 Geometry 1: Rectangular Box

To start, a simple case was made with no collimation or specialized shielding. This is given in Fig. 3.1. The geometry on Fig. 3.1 is a simple case that allows for a good baseline reference for dose and offers the benefit of spreading the required source activity along 8 sources. This baseline served as a good validation schema, as evidenced by the data given in chapter 2. This geometry offered the most homogenized flux, with a PTA value of 1.52; however, the required source activity and corresponding outside room dose was well above the desired range. This result disqualified some of the other proposed models, as they gave an even higher dose rate to the outside room.

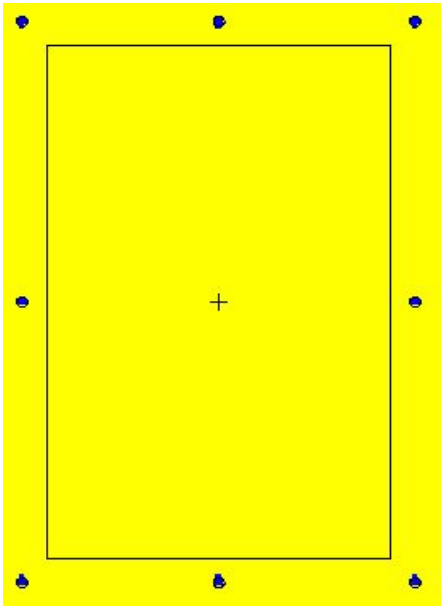

Figure 3.1: Eight sources arranged around rodent cages in rectangular formation. The lines surrounded by the eight blue sources indicate the rat cage boundaries.

3.1.2 Geometry 2: Collimated Rectangular Box

From the results in the preceeding geometry, it was clear that a reduction in dose to the outside room detector was necessary. Because of this, it was proposed to add collimators around each of the sources to increase the amount of 'useful' radiation entering the rodent cages and decrease the amount of radiation in the surrounding room. This geometry is graphed on Fig. 3.2.

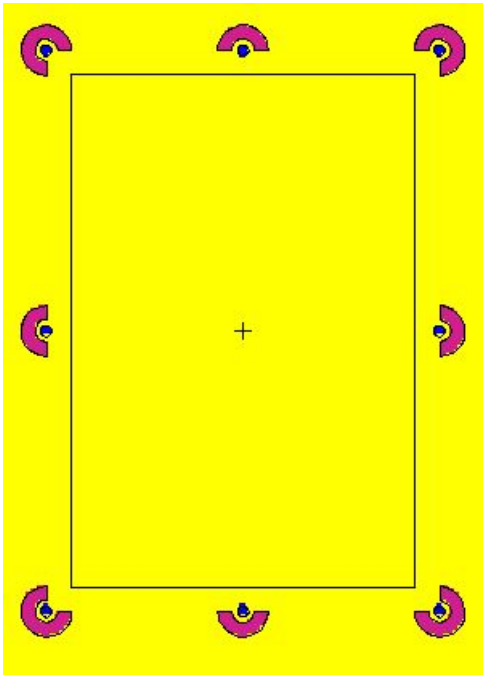

Figure 3.2: Eight collimated sources arranged around rodent cages in rectangular formation to reduce dose to outside room.

Initially tests done with lead were done using 2, 5, and 10 mm of lead. Dose rates did go down, but upon realizing the high cost of producing these shields, the shielding material was changed to sand. Shielding for sand was made to be in a 16 cm diameter cylinder. The increase in diameter was because the attenuation factor for sand is half that of lead. However, this geometry also had too high of a dose rate to the surrounding rooms.

3.1.3 Geometry 3: 6-source Collimated

This next iteration attempted to reduce the outside dose rate even further by reducing the number of sources and increasing the distance between the sources and

the wall with the highest dose rate(the closer east and west wall). This geometry (Fig. 3.3) was the most promising of the iterations, as it offered the most homogenized fluence rate across the rat cages by giving the lowest peak to average value. However, after numerous trials and shielding orientations and collimator designs, this design was unable to achieve a dose rate in the range of interest (2-4 mrem/hr) in the outside room.

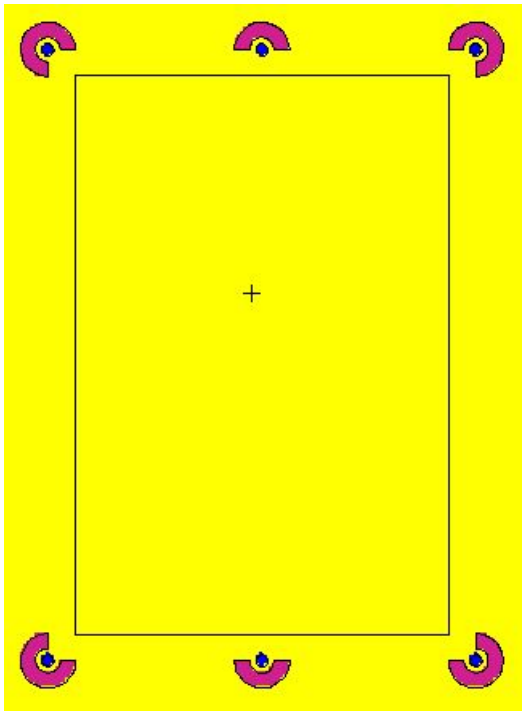

Figure 3.3: Two source removed geometry to decrease dose rate to outside room.

3.1.4 Geometry 4: Star Formation

The final permutation was meant to serve as a compromise between the balance of homogenized flux and outside dose rate, or alternatively, source number vs orien-

tation. To do this, a star geometry (Fig 3.4) was used.

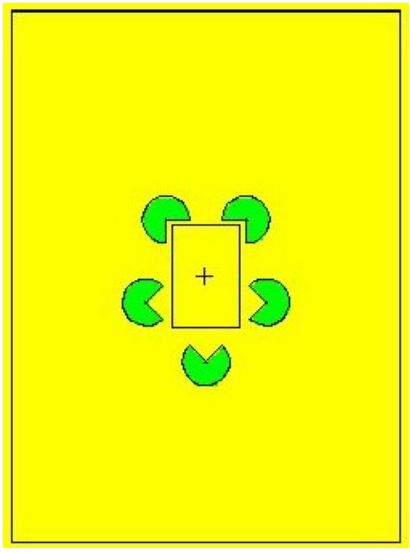

Figure 3.4: Star geometry of sources used to flatten the PTA inside of the rat cages.

This geometry gave exactly what was needed: a compromise between the PTA values and dose rate. The only modifications that had to be made were those designed to control the hotspots generated. This was achieved by moving two of the sources closer to the east and west walls. The shielding also had to be adapted to get the highest dose rate down from 6.04 mrem/hr down to around 3 mrem/hr. These critical modifications were incorporated into the final optimized star geometry formation.

3.1.5 Geometry 5: Optimized Star Formation

The star formation introduced in Fig. 3.4 gave slight asymmetries outside of the rat cage rack in the form of higher dose values at given locations, called 'hot-spots.'

These values were found by creating a mesh of detector cells along each of the walls to determine the exact locations of the hot-spots along the walls. This optimized source and room geometry is shown on Fig. 3.5.

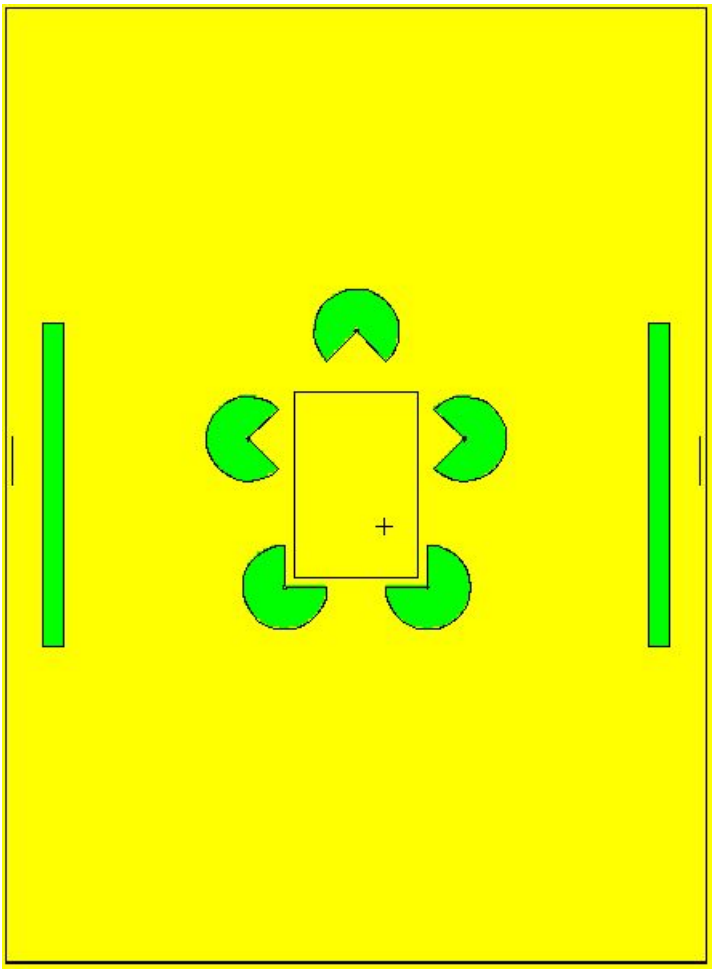

Figure 3.5: Optimal room design for irradiation experiments including shielding of hot-spots (green rectangles) and optimum PTA values. Additional thin lead shielding is placed behind the green rectangles to further shield the highest radiation spot.

The hot spot values were found by using a layered mesh detector along the wall with the highest dose rate (west wall.) The mesh detector response (Fig. 3.7) illustrates that there is a peak in dose at all depths in the wall just above coordinate system centerline. The optimized geometry seen on Fig 3.5 takes this into account and places a small lead shield over the hot spot zone. The addition of a sand wall just before the room wall was also necessary to drop the dose rate further along the wall to the acceptable range of around 2.5 mrem/hr.

3.2 Results from Each Geometry

Each geometry gave an advantage in PTA or dose rate. The results from geometries 1 through 3 demonstrated that a compromise had to be made between the two parameters. The star geometry gave the most promising results, assuming that the dose rate could be reduced. This was accomplished through the addition of shielding at the hotspots as well as an additional sand wall shield close to the wall. Hotspot shield effectiveness was confirmed through use of 'check detectors' which are displayed on Fig. 3.6. The detector with the highest response was evaluated before and after shielding. These data, along with the corresponding uncertainty, are given in Table 3.3 with all other pertinent data on Tables 3.1 and 3.2.

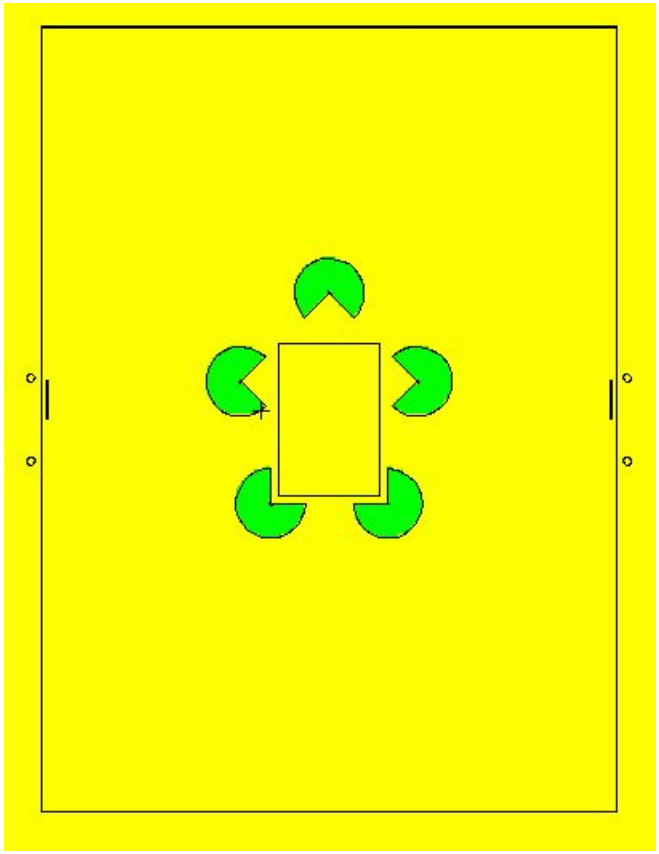

Figure 3.6: Optimal source orientation displaying 'check detectors' to verify hot-spot location along with effectivity of shielding.

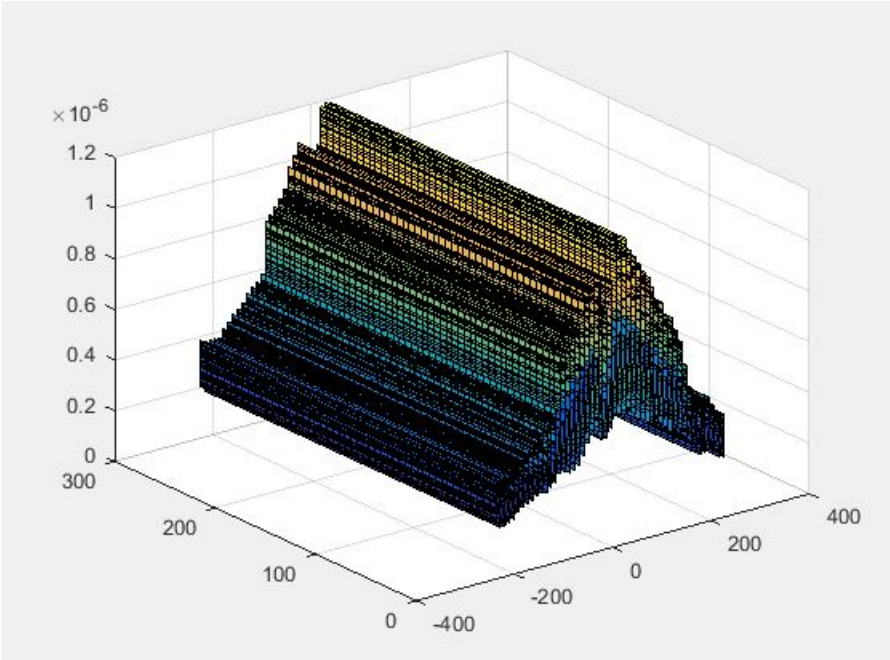

Figure 3.7: Wall surface mesh slices depicting spike in dose values at just above centerline.

It should be noted that the dose rates calculated in this model were using the maximum required activity to meet the required internal cage dose rate of 83 mrem/hr to ensure all rodents received the minimum experimental dose. Being that rodent dose was a function of the PTA, and the outside dose rate a function of the source orientation, this optimized star geometry was chosen. The data in Table 3.3 shows the shielded and un-shielded dose rate for the final optimal source geometry. They were shown to meet and/or exceed the requirements defined in the scope in the proceeding chapter, thus satisfying the objectives of this project.

Based on these data and results, the optimized star geometry is recommended for use in the irradiation of rodents. It met and exceeded all the requirements in ad-

Table 3.1: Dose data for each geometry and whether or not it was in the dose range of interest.

Geometry	Outside Room Fluence Rate (mrem/hr)	Statistical Uncertainty	Dose $\approx 2-4 mrem/hr$
8 Source Baseline	8.93	$> 2\%$	No
8 Source Collimated	7.10	3.20%	No
6 Source Collimated	7.35	3%	No
Star Source Collimated	6.04	1.42%	No
Optimized Star Source Collimated	3.01	$> 2\%$	Yes

Table 3.2: Fluence rate data obtained from each of the geometries.

Geometry	Peak-To-Average Fluence Rate	Required Activity/Max Fluence Rate	Statistical Uncertainty
8 Source Baseline	1.52	$8.29x10^9$	$> 2\%$
8 Source Collimated	1.58	$2.26x10^9$	3.20%
6 Source Collimated	1.14	$3.054x10^9$	3%
Star Source Collimated	1.60	$5.56x10^9$	1.42%
Optimized Star Source Collimated	1.60	$2.99x10^9$	$> 2\%$

Table 3.3: Final configuration dose values for shielded and non-shielded cases.

Detector Location	Non-Shielded $\dot{D}$ (mrem/hr)	Shielded $\dot{D}$ (mrem/hr)	Unc
North Wall	3.73	2.08	1.36%
South Wall	3.44	1.82	1.47%
East Wall	3.49	2.80	1.41%
West Wall	3.38	2.73	1.42%
Hot Spot:Highest	4.46	3.80	$> 2\%$

dition to offering a sand shielding arrangement with a relatively low cost that could be used in a myriad of arrangements, if the experiment should require it.

4. CONCLUDING STATEMENTS

When comparing the data with the requirements set by the experimenter those required to assure personnel safety, the choice that offered a relatively flat flux and a required dose-rate limit for the outside rooms was the star geometry. This geometry was also analyzed for its ability to generate hot-spots on the surrounding wall. These were located using a mesh detector and confirmed by analyzing the particle tracks and checking detector response at various locations in the outside room. After using these data, an optimized model was created that met all the requirements set for this project by allowing a compromise in peak-to-average fluence rate values and source orientation.

REFERENCES

[1] Forrest Brown and William Martin. Monte carlo methods for radiation transport analysis on vector computers. *Progress in Nuclear Energy*, 14(3):269–299, 1984.

[2] Eric Hall and Amato Giaccia. *Radiobiology for the Radiologist*. Lippincott Williams & Wilkins, 2006.

[3] John Hubbell and Stephen Seltzer. Tables of x-ray mass attenuation coefficients and mass energy-absorption coefficients 1 kev to 20 mev for elements z= 1 to 92 and 48 additional substances of dosimetric interest. Technical report, National Inst. of Standards and Technology-PL, Gaithersburg, MD (United States). Ionizing Radiation Div., 1995.

[4] Glenn Knoll. *Radiation detection and measurement*. John Wiley & Sons, 2010.

[5] R McConn Jr, Christopher Gesh, Richard Pagh, Robert Rucker, and R Williams III. Compendium of material composition data for radiation transport modeling. *PNNL-15870 Rev*, 1(4), 2011.

[6] J Kenneth Shultis, Richard Faw, and Kenneth Kase. *Radiation shielding*. Prentice Hall PTR, 1996.

[7] James Turner and Charles Kelsey. *Atoms, radiation, and radiation protection*. Wiley New York, 1995.

APPENDIX A

MCNP6.1 SOURCE CODE

```
Microgravity Rat Model w/ Star Source Geometry and hot spot shielding
C  80cm HIGH SHIELD
C   Added hot spot det, changed radius to see stats.
C
C  Model made by David Saucier
C    Texas A&M University
C    Department of Nuclear Engineering
C  VERSION DATE: 1/13/15
C Dev Note: The radius of the wire must be checked
C
C Cell Cards
100 102 -0.001225  -1  2  3 4 5 6 7
          #801 #802 #803 #804 #805 #103 #104
          IMP:P=1 $ Room Cell
101 102 -0.001225  -1 -2 510 511 512 513 514
                                515 516 517 518 VOL= 29e5
                                      IMP:P=1 $ Rat Carrier Cell
102 100 -11.342    -20 1 2 #103 IMP:P=1 $shielding
103 100 -11.342   (28 -27 21 -24  25 -26):(28 -27 -22 23 25 -26) IMP:P=1
104 1000 -1.7 (-32 33 -30 31 -37 36):(34 -35 -30 31 -37 36) IMP:P=1
C
C
800 101 -8.9 -1 2 -11 12  -3:-4:-5:-6:-7  IMP:P=1
C
C SAND COLUMATION Begin
801 1000 -1.7 3 100 -200 305 IMP:P=1
802 1000 -1.7 4  101 -201 304 IMP:P=1
803 1000 -1.7 5 102 -202 306 IMP:P=1
804 1000 -1.7 6 103 -203  (-302:-300) IMP:P=1
805 1000 -1.7 7 104 -204  (-302:301) IMP:P=1
C
C Begin Detector Cells
501 102 -0.001225 -501 IMP:P=1
502 102 -0.001225 -502 IMP:P=1
503 102 -0.001225 -503 IMP:P=1
504 102 -0.001225 -504 IMP:P=1
505 102 -0.001225  -505 IMP:P=1
C
C Begin Rat Cells
510 102 -0.001225 -510 IMP:P=1
511 102 -0.001225 -511 IMP:P=1
512 102 -0.001225 -512 IMP:P=1
513 102 -0.001225 -513 IMP:P=1
514 102 -0.001225 -514 IMP:P=1
515 102 -0.001225 -515 IMP:P=1
516 102 -0.001225 -516 IMP:P=1
517 102 -0.001225 -517 IMP:P=1
518 102 -0.001225 -518 IMP:P=1
C
C
```

```
C
C  Begin MISC detectors
600 102 -0.001225 -600 IMP:P=1
601 102 -0.001225 -601 IMP:P=1
602 102 -0.001225 -602 IMP:P=1
603 102 -0.001225 -603 IMP:P=1
C
C
998 102 -0.001225 1  2 501 502 503 504 505
          600 601 602 603 -999 20  IMP:P=1 $ Void Cell
999 0  1   20   999 IMP:P=0

C Surface Cards
C
C
1 RPP -173.19625 173.19625 -236.69625 236.69625 0 300 $Xray room boundary
2 RPP -30.48 30.48 -45.72 45.72 15.24 167.6400  $ Rat Cage
3 RCC -53.35 22.86 0.1     0 0 179  0.5
4 RCC  53.35 22.86 0.1    0 0 179  0.5
5 RCC  0 76.21 0.1          0 0 179 0.5
6 RCC  -35.50 -50.75 0.1      0 0 179 0.5
7 RCC 35.50 -50.75 0.1     0 0 179 0.5
11 PZ 180
12 PZ 0.1
C
C BEGIN Surface FOR 1/16" equivalent lead shielding
20 RPP -173.3549 173.3551 -236.855 236.855 0 300 $Lead Shielding
C
C  Hotspot Shielding---> For now, 3mm
21 PX -170.300
22 PX   170.300
23 PX   170.000
24 PX   -170.000
25 PY   0
26 PY   24
27 PZ  79.9
28 PZ  0
C Begin SAND SHIELDS
30  PY 80
31  PY -80
32  PX -145
33  PX  -155
34  PX   145
35  PX   155
36  PZ   0.001
37  PZ   180
C
C Begin Shielding iterations of 2, 4, 8, and 10 cm for doses
C MUST BE CHANGED FOR THIS FILE
C 50 RPP -150.2 150.2 -150.2 150.2 0 300
```

```
C 50 RPP -150.2 150.2 -150.2 150.2 0 300
C 51 RPP -150.4 150.4 -150.4 150.4 0 300
C 52 RPP -151.2 151.2 -151.2 151.2 0 300
C 53 RPP -152 152 -152 152 0 300
C
C BEGIN COLUMATION of the BEAMS
100 RCC -53.35 22.86 0.1     0 0 179  1
101 RCC  53.35 22.86 0.1    0 0 179  1
102 RCC  0 76.21 0.1          0 0 179 1
103 RCC  -35.50 -50.75 0.1      0 0 179 1
104 RCC 35.50 50.75 0.1     0 0 179 1
C
C The outer radius of columnators
C
200 RCC -53.35 22.86 0.1     0 0 179  21
201 RCC  53.35 22.86 0.1    0 0 179  21
202 RCC  0 76.21 0.1          0 0 179 21
203 RCC  -35.50 -50.75 0.1      0 0 179 21
204 RCC 35.50 -50.75 0.1     0 0 179 21
C
C Begin the plane slicing for corner columnation
300 px -35.51
301 px   35.51
302 py -50.76
303 py  22.87
304 WED 53.35 22.86 0.1 -22 22 0 -22 -22 0 0 0 179
305 WED -53.35 22.86 0.1 25 25 0 25 -25 0 0 0 179
306 WED 0 76.21 0.1  -25 -25 0 25 -25 0 0 0 179
C
C Detectors Outside Room
C  CHANGED TO +/-180 cm from 150 on E and W walls,
C     also changed radius to 3.5 cm. Special detector at hot spot
C
501  S     0.0    239.5   150  2.5  $Detector on N side of room
502  S     0.0   -239.5   150   2.5  $Detector on S side of room
503  S   180.0     0.0   150    3.5  $Detector on E side of room
504  S  -180.0    0.0   150     3.5  $Detector on W side of room
C
505  S   -178     14.21  81.00  2.5   $det at hot spot
C rat detectors
510 RCC   0  30.48 124  26 0 0 7
511 RCC   0   0       124  26 0 0 7
512 RCC   0  -30.48 124  26 0 0 7
513 RCC   0  30.48   84  26 0 0 7
514 RCC   0  0         84  26 0 0 7
515 RCC   0  -30.48 84  26 0 0 7
516 RCC   0  30.48  44  26 0 0 7
517 RCC   0    0      44  26 0 0 7
518 RCC   0  -30.48 44  26 0 0 7
C
```

```
C BEGIN MISC Detectors
600  S  -180 -25 75 2.5
601  S  -180  25 75 2.5
602  S   180 -25 75 2.5
603  S   180  25 75 2.5
C
999 so 99999

C Material Cards
C
mode p
C phys:p  $ 100 0 0 0 0 J 0
nps     5e8
print 110
C ptrac FILE=ASC
prdmp  1.0E7 2.0E7
C
C Begin Source Modelling- Complex
C Using Enclosing PPD Rejection Method
SDEF   X=d2 Y=d3 Z=d4 ERG=D1 PAR=2 CEL=800
SI1 L  1.1732 1.3325
SP1    0.9988 0.9988
SI2 -53.89 -52.80 -36 -34.98  -0.5 0.5 34.98 36  52.80 53.89
SP2 0  1  0 1 0 1  0  1  0 1
SI3 -51 -49.8 22 23 75 76.7
SP3 0  1  0 1 0 1
SI4 0 179
SP4 0 1
C
C Materials
C
M1    6000.84p   0.000150
        7000.84p   0.784429
        8000.84p   0.210750
       18000.84p   0.004671
M10     1000.84p   0.630489
        6000.84p   0.058149
        7000.84p   0.011680
        8000.84p   0.299682
M100   82000.84p   1.000000
M101   27060.84p       1.0
M102    1000.84p  -0.00453
        8000.84p  -0.5126
       14000.84p  -0.36036
       13000.84p  -0.03555
       11000.84p  -0.01527
       20000.84p  -0.05791
       26000.84p  -0.01378
C SAAAANNND
m1000  1000.84p   0.135405
```

```
C SAAAANNND
m1000  1000.84p   0.135405
            6000.84p    0.004874
            8000.84p    0.58389
           11000.84p    0.012932
           13000.84p    0.022215
           14000.84p    0.226483
           19000.84p    0.005179
           20000.84p    0.004874
           26000.84p    0.004146
C Photon Tally/s
FMESH74:p       GEOM=REC ORIGIN= -174.001  -236.8551  0
           IMESH= -174.00  -173.3551  IINTS= 0 1
           JMESH= -236.8550 236.8551   JINTS= 0 50
                KMESH= 0.1 300.1   KINTS= 0 50
FMESH84:p       GEOM=REC ORIGIN= 173.3550  -236.8551  0
           IMESH=  173.3551 174.00    IINTS= 0 1
           JMESH= -236.8550 236.8551   JINTS= 0 50
           KMESH= 0.1 300.1   KINTS= 0 50
f14:p  501 502 503 504
FC14    ANSI/ANS 6.1.11977 Flux-to-Dose Conversion outside Detectors
          (REM/hr)/(annihilation photon)/s
DE14    LOG
        0.01      0.03  0.05  0.07  0.1
        0.15      0.2   0.25  0.3   0.35
        0.4 0.45  0.5   0.55  0.6   0.65
        0.7 0.8   1     1.4   1.8
        2.2 2.6   2.8   3.25  3.75  4.25
        4.75      5     5.25  5.75  6.25
        6.75      7.5   9     11    13    15
DF14    LOG
        3.96E-06  5.82E-07    2.90E-07    2.58E-07
        2.83E-07  3.79E-07
        5.01E-07  6.31E-07    7.59E-07    8.78E-07
        9.85E-07  1.08E-06
        1.17E-06  1.27E-06    1.36E-06    1.44E-06
        1.52E-06  1.68E-06
        1.98E-06  2.51E-06    2.99E-06    3.42E-06
        3.82E-06  4.01E-06
        4.41E-06  4.83E-06    5.23E-06    5.60E-06
        5.80E-06  6.01E-06
        6.37E-06  6.74E-06    7.11E-06    7.66E-06
        8.77E-06  1.03E-05
        1.18E-05  1.33E-05
f24:p  101 510 511 512 513 514 515 516 517 518
FC24    ANSI/ANS 6.1.11977 Flux-to-Dose Conversion for Rats
          (REM/hr)/(annihilation photon)/s
DE24    LOG
        0.01      0.03  0.05  0.07  0.1
        0.15      0.2   0.25  0.3   0.35
```

```
          0.15      0.2   0.25  0.3   0.35
          0.4 0.45  0.5   0.55  0.6   0.65
          0.7 0.8   1     1.4   1.8
          2.2 2.6   2.8   3.25  3.75  4.25
          4.75      5     5.25  5.75  6.25
          6.75      7.5   9     11    13    15
DF24      LOG
          3.96E-06  5.82E-07    2.90E-07    2.58E-07
          2.83E-07  3.79E-07
          5.01E-07  6.31E-07    7.59E-07    8.78E-07
          9.85E-07  1.08E-06
          1.17E-06  1.27E-06    1.36E-06    1.44E-06
          1.52E-06  1.68E-06
          1.98E-06  2.51E-06    2.99E-06    3.42E-06
          3.82E-06  4.01E-06
          4.41E-06  4.83E-06    5.23E-06    5.60E-06
          5.80E-06  6.01E-06
          6.37E-06  6.74E-06    7.11E-06    7.66E-06
          8.77E-06  1.03E-05
          1.18E-05  1.33E-05
f34:p  501 502 503 504
f44:p  101 510 511 512 513 514 515 516 517 518
F104:p 505 600 601 602 603
FC104     ANSI/ANS 6.1.11977 Flux-to-Dose Conversion outside Detectors
            (REM/hr)/(annihilation photon)/s HOT SPOT
DE104     LOG
          0.01      0.03  0.05  0.07  0.1
          0.15      0.2   0.25  0.3   0.35
          0.4 0.45  0.5   0.55  0.6   0.65
          0.7 0.8   1     1.4   1.8
          2.2 2.6   2.8   3.25  3.75  4.25
          4.75      5     5.25  5.75  6.25
          6.75      7.5   9     11    13    15
DF104     LOG
          3.96E-06  5.82E-07    2.90E-07    2.58E-07
          2.83E-07  3.79E-07
          5.01E-07  6.31E-07    7.59E-07    8.78E-07
          9.85E-07  1.08E-06
          1.17E-06  1.27E-06    1.36E-06    1.44E-06
          1.52E-06  1.68E-06
          1.98E-06  2.51E-06    2.99E-06    3.42E-06
          3.82E-06  4.01E-06
          4.41E-06  4.83E-06    5.23E-06    5.60E-06
          5.80E-06  6.01E-06
          6.37E-06  6.74E-06    7.11E-06    7.66E-06
          8.77E-06  1.03E-05
          1.18E-05  1.33E-05
```